Effect of Impedance-Shaping on Perception of Soft Tissues in Macro-Micro Teleoperation

Hyoung Il Son, *Member, IEEE*, Tapomayukh Bhattacharjee, and Hideki Hashimoto, *Fellow, IEEE*

***Abstract*—This paper aims at analyzing the effect of widely known impedance-shaping (IS) control method on the perception of soft tissues in telemicrosurgical applications. The generalized teleoperation control architecture has been modified to include the IS term. New performance index has been defined based on the two proposed indices for the detection and the discrimination of the soft environments to analyze the effect of this modified control on the kinesthetic perception of soft tissues. The effect is then theoretically analyzed on the conventional position–position, force–position, and four-channel control architectures based on the newly defined index. The effectiveness of this newly proposed kinesthetic perception index is also verified using psychophysics experiments. The theoretical analysis of the effects of the IS method on the perception of soft tissues is then validated using the proposed index by experiments with phantom soft tissues for conventional teleoperation architectures.**

***Index Terms*—Impedance shaping (IS), kinesthetic perception, psychophysics, soft tissue, teleoperation.**

I. Introduction

TELESURGERY has mainly been depending on visual information for its success until now. However, many studies have shown that additional force-feedback information can increase the performance and efficiency of telesurgical operations [1], [2]. In particular, internal injuries and/or trauma can be minimized by enhancing the surgeon's ability to detect different tissues and feel the differences among various tissues [3], [4]. This type of capability gains more importance during instances of telemicrosurgery because of the small magnitude of force reflection involved in such procedures.

A macro-micro teleoperation system, as illustrated in Fig. 1, is generally used to increase the positioning accuracy of surgical tools and enhance the sensation transferred to the operator [5], [6]. The mechanism of the master [7] and the slave manipulator [8] is a critical factor in increasing the positioning accuracy [9], [10]. There have been many studies on enhancing the sensation of the remote operator for effective telesurgical operations through various control design strategies. Effects of position and force scaling on human perception have been investigated in other studies [11]–[15]. Bilateral control with IS was originally proposed as a means of altering the impedance of a task [11]. Kobayashi [12] showed that time scaling should be considered to allow perception of physically ideal environment in the scaled teleoperation. Nonlinear force mapping was proposed by Malysz and Sirouspour [13] for improved discrimination of the environment stiffness in telemanipulation systems. Recently, Botturi *et al.* [14] presented experiments on human subjects, which showed enhanced perception by suitable scaling. Yamakawa *et al.* [15] empirically found necessary conditions for selecting the force-scaling ratio. Scaled telemanipulation systems have also been dealt in [16] wherein a model reference adaptive controller has been used to compensate friction forces so that proper force information is received in the master side. Katsura *et al.* proposed a method for force reflection based on disturbance observer in multilateral control systems [17] and a twin-robot-based environment quarrier method [18], which can increase the bandwidth of force information, and also designed the multilateral controller based on modal decomposition in which the scaling factors can be chosen as per the requirement of haptic applications [19]. Shimono *et al.* came up with an idea of abstraction, reconstruction, and reproduction of environment forces to store the bilateral force sensation for transmission purposes [20]. Slama *et al.* analyzed the effects of force and motion scaling in teleoperation systems under the effect of variable transmission time delays and packet losses [21]. An approach based on the distributed construction of configuration spaces is presented in [22] for effective haptic perception in human–computer interaction. Yalcin and Ohnishi attempted to considerably improve the transparency and perception bandwidth of teleoperation systems with the help of proper motion and force scaling and by using direct acceleration waves in [23].

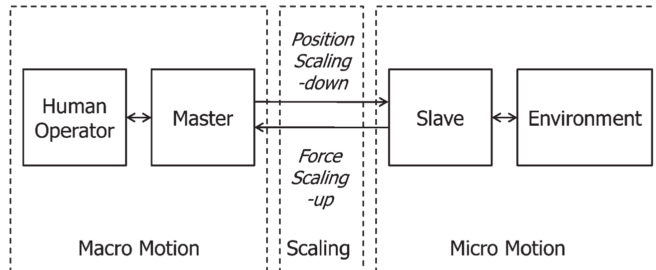

Fig. 1. Macro-micro teleoperation system.

Manuscript received March 1, 2010; revised July 21, 2010 and March 6, 2011; accepted April 20, 2011. Date of publication May 2, 2011; date of current version March 30, 2012. This paper was presented in part at the IEEE Engineering Medicine and Biology Conference, Vancouver, BC, Canada, August 20–24, 2008, and at the International Conference on Robotics and Automation, Anchorage, AK, May 3–8, 2010.

H. I. Son is with the Department of Human Perception, Cognition and Action, Max Planck Institute for Biological Cybernetics, 72076 Tübingen, Germany (e-mail: hyoungil.son@tuebingen.mpg.de).

T. Bhattacharjee is with the Center for Cognitive Robotics Research, Korea Institute of Science and Technology, Seoul 136-791, Korea (e-mail: tapomayukh_kaist@kaist.ac.kr).

H. Hashimoto is with the Institute of Industrial Science, The University of Tokyo, Tokyo 153-8505, Japan (e-mail: hashimoto@iis.u-tokyo.ac.jp).

Color versions of one or more of the figures in this paper are available online at http://ieeexplore.ieee.org.

Digital Object Identifier 10.1109/TIE.2011.2148672

In addition to the performance enhancement, the stability aspect is also important, and it is affected by the scaling factors in the macro-micro teleoperation system. Poorten *et al.* proposed a robust control for fixed-scaled teleoperation [24] and variably scaled teleoperation [25]. The implications of scaling on the stability of a loop-shaping teleoperation system were reported in [26]. Boukhnifer and Ferreira [27] developed an H_∞ loop-shaping bilateral control to ensure stability robustness against time delays and variation of force-scaling factors.

All of the aforementioned studies agree on one common aspect that the impedance-shaping (IS) method is a suitable method to enhance the perception of the remote operator in teleoperation applications. Hence, in this paper, the effect of the IS control method on the human operator's perception of soft tissues is analyzed using the generalized teleoperation control which is modified to accommodate the IS term.

Quantitative performance indices are necessary to gauge the enhancement of the remote human operator sensation through the various control methods, and hence, there have also been some related works on defining suitable indices. Cavusoglu *et al.* [3] defined a performance measure of fidelity as the sensitivity of the transmitted impedance to changes in the environment impedance. They argued that fidelity is a more important design objective than transparency [28] in surgical applications. Gersem *et al.* [4] enhanced the perception of stiffness by optimizing a bilateral controller to increase the relative changes. Their method is based on the just noticeable difference (JND) [29], [30]. Control optimization for improved fidelity of haptic feedback was implemented by estimating the impedance of the remote environment [31]. Hirche and Buss [32] and Hinterseer *et al.* [33] exploited the perceptual property to reduce the amount of transmission data in teleoperation. Experiments involving human subjects have been performed to explore whether force measurements can be useful in improving the performance of tasks such as soft-tissue palpation and discrimination of tissue stiffness [34]. This paper, however, exploits a new performance index based on psychophysics to quantify the kinesthetic perception. The new performance index ranges from zero, representing no sensation, to unity, representing perfect perception. This new index is based on the newly proposed metrics of detection ability and discrimination ability [35], [36]. It should be noted that, at this point, the proposed metric has been used for designing new controllers for teleoperation systems previously [36], and the efficacy of this index has been verified and the performance of the controller has been validated by comparing the developed controller with that of the methods proposed in [3] and [13].

This paper, hence, uses the newly developed index of kinesthetic perception and analyzes the effect of IS on the operator's perception using the developed index. This is achieved by developing a new IS term and then modifying the generalized teleoperation architecture by including this term in the control architecture. The performance of the modified teleoperation control architecture in enhancing the perception of soft tissues in macro-micro-scaled teleoperation systems is then analyzed for position–position (PP), force–position (FP), and four-channel (4C) controllers. The effectiveness of the newly developed perception index is also verified by performing psychophysics experiments. The previous theoretical analyses are further verified using subsequent experiments with a master–slave system interacting with phantom soft tissues.

II. Impedance-Shaping

A. Impedance-Shaping in Scaled Teleoperation

This paper considers the following scaling law for the typical macro-micro teleoperation system shown in Fig. 1:

$$x_s = S_p x_m \quad f_m = S_f f_s. \tag{1}$$

Here, f_m, x_m, f_s, and x_s are the force of the master, the position of the master, the force of the slave, and the position of the slave, respectively. The position-scaling factor and force-scaling factor are defined as S_p and S_f, respectively.

The position-scaling factor S_p is simply considered to be the inverse value of the ratio of an index length, i.e., the geometrical scaling, between the macro master side and the micro slave side. Thus, S_p is less than one in the macro-micro teleoperation illustrated in Fig. 1. The selection of the force-scaling factor is a more complicated problem because, if S_f is selected as a certain constant value, it becomes impossible to scale simultaneously the inertial force, viscous force, and stiff force together properly [10]–[12]. This issue is explained in terms of geometric similarity and dynamic similarity [37]. As geometric similarity requires that the length ratios on the master side are in constant proportion to those on the slave side, the aforementioned selection of S_p can satisfy the geometric similarity requirement. Dynamic similarity, however, requires consistency in the dynamic equations that describe the behavior on the master/slave side; therefore, the constant S_f cannot satisfy the dynamic similarity requirement because the physical phenomena, i.e., inertial force, viscous force, and stiff force, scale differently with length. The operator, generally, should work in a magnified microenvironment with a scale appropriate for manipulation with minimal distortion of environment information such as inertia and viscosity. One method to accomplish this issue is to apply impedance scaling to reshape the environment impedance [11].

To increase the dexterity of the micromanipulation, the IS method reshapes the impedance transmitted to the master side by adding an IS compensator which is designed to have particular inertia, viscosity, and stiffness terms. It is very important to know how physical phenomena change when the position is scaled and to know which physical phenomena are dominant in the environment to design the IS compensator properly. This paper assumes that inertia, viscosity, and stiffness are functions of $(length)^3$, $(length)^2$, and $(length)^2$, respectively [11], [12], [16], [37]. Hence, the design procedure of the IS compensator is given as follows:

$$\begin{aligned} m_{\text{scaling}} &= \upsilon \left(\frac{1}{S_p}\right)^3 m_{\text{original}} \\ b_{\text{scaling}} &= \nu \left(\frac{1}{S_p}\right)^2 b_{\text{original}} \\ k_{\text{scaling}} &= \kappa \left(\frac{1}{S_p}\right)^2 k_{\text{original}}. \end{aligned} \tag{2}$$

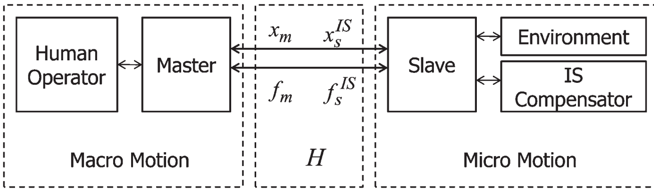

Fig. 2. Macro-micro teleoperation system with IS.

Here, m_{original}, b_{original}, and k_{original} are the inertia, viscosity, and stiffness coefficients of the original system, respectively. The variables m_{scaling}, b_{scaling}, and k_{scaling} denote those of the scaled system; and υ, ν, and κ are the design parameters for the IS step. The environment impedance can be modeled as the second-order linear time-invariant (LTI) model

$$Z_e = m_e s^2 + b_e s + k_e \tag{3}$$

where m_e, b_e, and k_e are, respectively, the inertia, viscosity, and stiffness coefficients of the microenvironment. The impedance of the scaled environment with impedance shaping based on (2) is as follows:

$$Z_{e,\text{scaling}}^{\text{IS}} = \upsilon \left(\frac{1}{S_p}\right)^3 m_e s^2 + \nu \left(\frac{1}{S_p}\right)^2 b_e s + \kappa \left(\frac{1}{S_p}\right)^2 k_e. \tag{4}$$

Thus, $Z_{e,\text{scaling}}^{\text{IS}}$ is formulated as

$$Z_{e,\text{scaling}}^{\text{IS}} = \frac{1}{S_p} Z_{e,\text{original}}^{\text{IS}} = \frac{1}{S_p}\left(Z_e + Z_c^{\text{IS}}\right) \tag{5}$$

where $Z_{e,\text{original}}^{\text{IS}}$ is the impedance of the original (micro) environment with IS and Z_c^{IS} denotes the IS compensator. Therefore, the IS compensator is designed as

$$\begin{aligned} Z_c^{\text{IS}} &= S_p Z_{e,\text{scaling}}^{\text{IS}} - Z_e \\ &= \upsilon \left(\left(\frac{1}{S_p}\right)^2 - 1\right) m_e s^2 + \nu \left(\frac{1}{S_p} - 1\right) b_e s \\ &\quad + \kappa \left(\frac{1}{S_p} - 1\right) k_e. \end{aligned} \tag{6}$$

The design parameters for IS, υ, ν, and κ are selected to optimize the performance index for kinesthetic perception. This paper, for example, considers the parameters as unity.

B. Control Architecture

Fig. 2 shows a macro-micro teleoperation system with the IS compensator. The compensated position and the force of the environment are referred as x_s^{IS} and f_s^{IS}, respectively. An input–output relationship between the positions and forces of the master and slave is defined using a hybrid matrix [38] which is referred to as H in

$$\begin{bmatrix} f_m \\ -x_s^{\text{IS}} \end{bmatrix} = H \begin{bmatrix} x_m \\ f_s^{\text{IS}} \end{bmatrix} = \begin{bmatrix} h_{11} & h_{12} \\ h_{21} & h_{22} \end{bmatrix} \begin{bmatrix} x_m \\ f_s^{\text{IS}} \end{bmatrix}. \tag{7}$$

The generalized 4C control architecture [28] is applied to a macro-micro teleoperation system with the IS shown in Fig. 2. The resultant control is as illustrated in Fig. 3. In this case, H is obtained from Fig. 3 using the second-order LTI dynamic model of the master Z_m, the slave Z_s, and controllers C_i, $i = m, c, 1, \ldots, 6$. H is identical to the hybrid matrix of the generalized 4C control architecture without IS because H represents associations of x_m and f_m with x_s^{IS} and f_s^{IS}, respectively, and not with x_s and f_s. Hence, for simple notation, H is also used to represent the hybrid matrix of the generalized 4C control architecture without IS

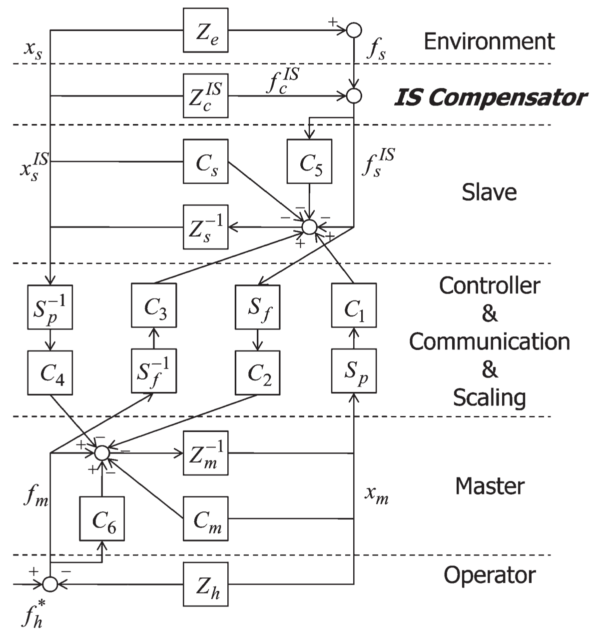

Fig. 3. Generalized and scaled 4C control architecture with IS.

$$H = \begin{bmatrix} \frac{Z_{cm}Z_{cs}+C_1C_4}{(1+C_6)Z_{cs}-S_p^{-1}S_f^{-1}C_3C_4} & \frac{S_fC_2Z_{cs}-S_p^{-1}C_4(1+C_5)}{(1+C_6)Z_{cs}-S_p^{-1}S_f^{-1}C_3C_4} \\ \frac{-S_f^{-1}C_3Z_{cm}-S_pC_1(1+C_6)}{(1+C_6)Z_{cs}-S_p^{-1}S_f^{-1}C_3C_4} & \frac{(1+C_5)(1+C_6)-C_2C_3}{(1+C_6)Z_{cs}-S_p^{-1}S_f^{-1}C_3C_4} \end{bmatrix}. \tag{8}$$

Here, C_1 is the feedforward position control to the slave, C_2 is the feedforward force gain to the master, C_3 is the feedforward force gain to the slave, C_4 is the feedforward position control to the master, C_5 is the local force gain in the slave, C_6 is the local force gain in the master, C_m is the local position control in the master, and C_s is the local position control in the slave. Z_{cm} and Z_{cs} are defined as $Z_{cm} = Z_m + C_m$ and $Z_{cs} = Z_s + C_s$ for simple expression of the equation. The human intended-force input is expressed as f_h^*.

III. Kinesthetic Perception

Quantitative analysis of the effects of IS control is necessary, and hence, a newly developed index of kinesthetic perception is proposed which can serve as a metric for judging the effectiveness of the IS method in enhancing the perception of soft tissues for the conventional teleoperation control architectures.

A. Kinesthetic Perception Region

Human perception can be categorized by normally two types of thresholds such as the detection and the discrimination of a kinesthetic stimulus (ϕ) [29]. First, the absolute threshold (AL for *absolute limen*) is defined as the smallest amount of stimulus required to produce a sensation in a detection task. A detectable stimulus based on AL can be represented as follows:

$$\phi_{\text{detectable}} = \{\phi_k | \forall k > 0, \phi_k \geq AL\}. \tag{9}$$

The second is the difference threshold (DL for *difference limen*) which can be defined as the smallest amount of stimulus change required to produce a change in the sensation of a discrimination task. The DL and the stimulus intensity generally have a linear relationship which is popularly known as the Weber's law. It is defined as in

$$c = \frac{\Delta\phi}{\phi_0} = \frac{DL}{\phi_0}. \tag{10}$$

Here, ϕ_0 is the initial intensity of the stimulus, $\Delta\phi$ is the smallest discriminable change of the stimulus intensity, and the constant c is the Weber's fraction. The constant c, in many studies, is also referred to as the JND. Equation (11) shows the range of stimuli which can be discriminated from the initial intensity based on the concept of the JND

$$\phi_{\text{discriminable}} = \{\phi_k | \forall k > 0, \phi_k \geq (1 + JND)\phi_0 \\ \text{or } \phi_k \leq (1 - JND)\phi_0\}. \tag{11}$$

Accordingly, this paper refers to the detection threshold and the discrimination threshold as the AL and the JND, respectively. The lower the AL and the JND values, the easier it is to detect and discriminate relatively.

In telesurgery, the impedance (Z) is one of the most important stimuli for perceiving dynamic changes in the environment. This measure contains information about changes in the position, force, and mechanical properties, including the stiffness, viscosity, and inertia. Accurate perception of the mechanical properties is, therefore, important in an environment composed of internal organs and tissues. Hence, the impedance Z_{to}, which is transmitted to the operator through the master and slave system, has to fall into the region that satisfies (9) and (11) to perceive the environment accurately. This region is referred to as the kinesthetic perception region, as shown in Fig. 4. The x-axis denotes the initial intensity of the impedance while the y-axis shows the secondary intensity of the impedance at some point in the future. The kinesthetic perception capabilities are, therefore, enhanced by enlarging the kinesthetic perception region quantitatively.

B. Performance Index

It is necessary to define a performance index to quantitatively compare the kinesthetic perception for different control architectures. First, a metric for each enhancement method for kinesthetic perception is defined quantitatively using a 2-norm operation as follows:

1) Metric for the Detection Ability:

$$M_{\text{detection}} = \left\| W_s \frac{Z_{to}}{Z_e} \bigg|_{Z_e = \tilde{Z}_e} \right\|_2. \tag{12}$$

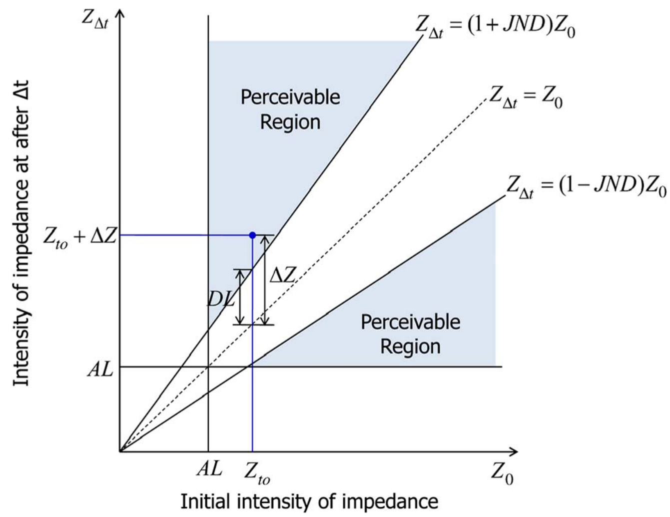

Fig. 4. Kinesthetic perception region.

2) Metric for the Discrimination Ability:

$$M_{\text{discrimination}} = \left\| W_s \frac{\Delta Z_{to}/Z_{to}}{\Delta Z_e/Z_e} \bigg|_{Z_e = \tilde{Z}_e} \right\|_2. \tag{13}$$

Here, W_s is a low-pass weighting function. This function is defined because a human cannot perceive kinesthetic stimuli at high frequencies [30], [35]. In addition, $\tilde{Z}_e$ denotes the nominal environment impedance.

Metrics for the detection and the discrimination enhancement methods indicate the detection and the discrimination abilities, respectively. $M_{\text{detection}}$ and $M_{\text{discrimination}}$ will be equal to one in the case of a perfect transparent teleoperation system. The detection ability will be increased, i.e., the detection threshold decreases, if $M_{\text{detection}}$ is larger than one. The case in which $M_{\text{discrimination}} > 1$ also implies an increase in the discrimination ability, i.e., a decrease of the detection threshold. Theoretically, $M_{\text{detection}} = M_{\text{discrimination}} = 0$ indicates no detection and discrimination ability, i.e., it suggests that the operator cannot perceive any environment, and $M_{\text{detection}} = M_{\text{discrimination}} = \infty$ represents a case in which perfect detection and discrimination abilities exist, i.e., the operator can perceive any environment.

The target performance index for kinesthetic perception can be defined as the shaded area shown in Fig. 4. This is also shown in (14). In this context, we argue that the performance index developed in [3] is based on the concept of fidelity which measures the sensitivity of the transmitted impedance to changes in the environmental impedance and is different from the concept of DL. According to Weber's law, the DL varies with the initial intensity of impedance, and therefore, we claim that it might be more appropriate to use our proposed criterion which measures the sensitivity of the relative change of the transmitted impedance to relative changes in the environment impedance for enhancing the discrimination ability or the JND. This is because our focus is toward enhancing surgeon's perception capabilities which, we believe, is very essential for a successful telesurgical procedure where human is in the loop. This reason for using our proposed index can be further bolstered by the fact

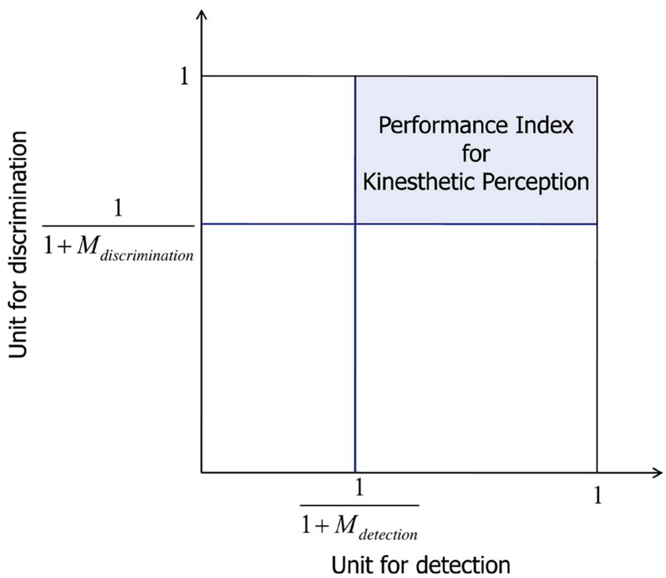

Fig. 5. Performance index for kinesthetic perception.

that the enhancement of detection and discrimination abilities, using their approach, is much less when compared to our perception-optimized control scheme as is evident from the experimental results [36]. In addition, their work does not help to increase the detection ability for environment with very small impedance like that of microsurgical applications as is evident from the results [36]. The detailed comparison results can be seen in our previous work [36].

3) Performance Index for Kinesthetic Perception:

$$\begin{aligned}\mathrm{PI}_{\mathrm{perception}} &= \text{Area of Quantified Kinesthetic Perception Region}\\ &= \left(1-\frac{1}{1+M_{\mathrm{detection}}}\right)\\ &\quad\cdot\left(1-\frac{1}{1+M_{\mathrm{discrimination}}}\right)\\ &= (1-M_1)\cdot(1-M_2).\end{aligned} \tag{14}$$

The performance index is defined as a combination of $M_{\mathrm{detection}}$ and $M_{\mathrm{discrimination}}$ to represent the kinesthetic perception region quantitatively. Fig. 5 is mapped from Fig. 4 by scaling the performance index to unity for perfect kinesthetic perception, which implies that the operator can detect any magnitude of environmental impedance and can discriminate any changes in environmental impedance. For the perfect transparent system, $\mathrm{PI}_{\mathrm{perception}}$ becomes 0.25. In the case of no detection ability or no discrimination ability, theoretically, $\mathrm{PI}_{\mathrm{perception}}$ becomes zero, i.e., no perception ability, even if the discrimination ability is perfect ($M_{\mathrm{discrimination}} = \infty$) or if the detection ability is perfect ($M_{\mathrm{detection}} = \infty$). Practically, however, a case with neither perception ability nor discrimination ability cannot occur.

IV. Analysis of the Effect of Impedance-Shaping

A. Kinesthetic Perception Analysis

The hybrid matrix with IS H^{IS}, as defined in (15), is formulated in the form of the hybrid matrix H to analyze the enhancement of the transmitted impedance to the operator in a range from "without IS" to "with IS"

$$\begin{bmatrix} f_m \\ -x_s \end{bmatrix} = H^{\mathrm{IS}}\begin{bmatrix} x_m \\ f_s \end{bmatrix} = \begin{bmatrix} h_{11}^{\mathrm{IS}} & h_{12}^{\mathrm{IS}} \\ h_{21}^{\mathrm{IS}} & h_{22}^{\mathrm{IS}} \end{bmatrix}\begin{bmatrix} x_m \\ f_s \end{bmatrix}. \tag{15}$$

First, f_s^{IS} is replaced with $f_s + Z_c^{\mathrm{IS}} x_s$ in (7) from the relationships $f_s^{\mathrm{IS}} = f_s + f_c^{\mathrm{IS}}$ and $f_c^{\mathrm{IS}} = Z_c^{\mathrm{IS}} x_s$. As x_s^{IS} is equal to x_s, (7) is simply formulated as follows:

$$\begin{aligned}\begin{bmatrix} f_m \\ -x_s \end{bmatrix} &= \frac{1}{1+h_{22}Z_c^{\mathrm{IS}}}\\ &\quad\times\begin{bmatrix} h_{11}+(h_{11}h_{22}-h_{12}h_{21})Z_c^{\mathrm{IS}} & h_{12} \\ h_{21} & h_{22}\end{bmatrix}\begin{bmatrix} x_m \\ f_s \end{bmatrix}\\ &= \frac{1}{1+h_{22}Z_c^{\mathrm{IS}}}\begin{bmatrix} h'_{11} & h_{12} \\ h_{21} & h_{22}\end{bmatrix}\begin{bmatrix} x_m \\ f_s \end{bmatrix}\\ &= \begin{bmatrix} h_{11}^{\mathrm{IS}} & h_{12}^{\mathrm{IS}} \\ h_{21}^{\mathrm{IS}} & h_{22}^{\mathrm{IS}} \end{bmatrix}\begin{bmatrix} x_m \\ f_s \end{bmatrix}\\ &= H^{\mathrm{IS}}\begin{bmatrix} x_m \\ f_s \end{bmatrix}.\end{aligned} \tag{16}$$

The impedance transmitted to the operator for the control architecture without IS is obtained as shown in (17) at the bottom of the page. Moreover, the transmitted impedance to the operator with IS is derived as (18) using (16) and (17)

$$\begin{aligned}Z_{to}^{\mathrm{IS}} &= \frac{h_{11}^{\mathrm{IS}} + \left(h_{11}^{\mathrm{IS}}h_{22}^{\mathrm{IS}} - h_{12}^{\mathrm{IS}}h_{21}^{\mathrm{IS}}\right)Z_e}{1+h_{22}^{\mathrm{IS}}Z_e}\\ &= \frac{h'_{11}\left(1+h_{22}Z_c^{\mathrm{IS}}\right) + \left(h'_{11}h_{22}-h_{12}h_{21}\right)Z_e}{\left(1+h_{22}Z_c^{\mathrm{IS}}\right)\left[1+h_{22}\left(Z_e+Z_c^{\mathrm{IS}}\right)\right]}.\end{aligned} \tag{18}$$

Finally, the enhancement of the transmitted impedance to the operator from "without IS" to "with IS" is analyzed by comparing Z_{to} and Z_{to}^{IS} as defined in (17) and (18), respectively. The compared result is shown in (19) and is represented hereinafter in more detail for the case of widely used two-channel control architectures

$$\begin{aligned}Z_{to}^{\mathrm{IS}} - Z_{to} &= \frac{h'_{11}\left(1+h_{22}Z_c^{\mathrm{IS}}\right) + \left(h'_{11}h_{22}-h_{12}h_{21}\right)Z_e}{\left(1+h_{22}Z_c^{\mathrm{IS}}\right)\left[1+h_{22}\left(Z_c^{\mathrm{IS}}+Z_e\right)\right]}\\ &\quad-\frac{h_{11}+(h_{11}h_{22}-h_{12}h_{21})Z_e}{1+h_{22}Z_e}\\ &= \frac{-\left(Z_c^{\mathrm{IS}}+h_{12}h_{21}\right)}{\left(1+h_{22}Z_e\right)\left[1+h_{22}\left(Z_c^{\mathrm{IS}}+Z_e\right)\right]}.\end{aligned} \tag{19}$$

1) PP Control Architecture: PP control architecture is an architecture in which only the position information is transmitted

$$Z_{to} = \frac{h_{11}+(h_{11}h_{22}-h_{12}h_{21})Z_e}{1+h_{22}Z_e} = \frac{Z_{cm}Z_{cs}+C_1C_4+\left[(1+C_5)Z_{cm}+S_pS_fC_1C_2\right]Z_e}{(1+C_6)-S_p^{-1}S_f^{-1}C_3C_4+\left[(1+C_5)(1+C_6)-C_2C_3\right]Z_e} \tag{17}$$

between the master and the slave, i.e., $C_2 = C_3 = 0$. The hybrid matrix for PP control architecture can be derived from (8)

$$H = \begin{bmatrix} \frac{Z_{cm}Z_{cs}+C_1C_4}{(1+C_6)Z_{cs}} & \frac{-S_p^{-1}C_4(1+C_5)}{(1+C_6)Z_{cs}} \\ \frac{-S_pC_1}{Z_{cs}} & \frac{1+C_5}{Z_{cs}} \end{bmatrix}. \tag{20}$$

Generally, local force control gains C_5 and C_6 are designed as $-1 \leq C_5$ and $C_6 \leq 1$; hence, $h_{22} = (1 + C_5)/Z_{cs} \geq 0$ is obtained. In addition, $h_{12}h_{21}$ is derived by

$$h_{12}h_{21} = \frac{C_1C_4(1+C_5)}{(1+C_6)(Z_{cs})^2}. \tag{21}$$

The equation $h_{12}h_{21} < 0$ is satisfied because C_1 and C_4 are designed as C_s and $-C_m$, respectively, based on transparency-optimized control law [28]. For the PP controller, $Z_{to}^{\mathrm{IS}} - Z_{to}$ is larger than zero.

2) FP Control Architecture: The control architecture in which only the position information is transmitted from the master to the slave and the force information is fed back from the slave to the master, i.e., $C_3 = C_4 = 0$, is termed FP control architecture. Equation (22) expresses the hybrid matrix of the FP control architecture

$$H = \begin{bmatrix} \frac{Z_{cm}}{1+C_6} & \frac{S_fC_2}{1+C_6} \\ \frac{-S_pC_1}{Z_{cs}} & \frac{1+C_5}{Z_{cs}} \end{bmatrix}. \tag{22}$$

It is simply observed that $h_{22} \geq 0$ and $h_{12}h_{21} < 0$ from (22), as explained in the case of the PP controller. The value of Z_{to}^{IS} also increases compared to Z_{to}.

In summary, $Z_{to}^{\mathrm{IS}} - Z_{to}$ is generally larger than zero because $h_{12}h_{21} < 0$ and $h_{22} \geq 0$. The impedance transmitted to the operator is enhanced with the help of IS; therefore, the detection threshold can be decreased using IS. If the teleoperation system becomes more transparent, the decrease of the detection threshold becomes $Z_{to}/(Z_c^{\mathrm{IS}} + Z_{to})$.

Please note that the difference between Z_{to} and Z_{to}^{IS} is calculated because when the difference in the metric for the detection ability is analyzed, it boils down to the difference between Z_{to} and Z_{to}^{IS} in the numerator with the denominator as Z_e, and hence, the numerator becomes the deciding factor. In the case of discrimination ability, however, we could not analyze the effect of IS on the discrimination ability because it is very complex and difficult to calculate the enhancement of the relative change of the transmitted impedance, i.e., $(\Delta Z_{to}^{\mathrm{IS}}/Z_{to}^{\mathrm{IS}}) - (\Delta Z_{to}/Z_{to})$, analytically because ΔZ cannot be formulated in the form of a hybrid matrix.

B. Stability Analysis

It is well known that the product of scaling factors S_pS_f affects the stability of a macro-micro teleoperation system [25]–[27]. Position and force scaling factors are defined so as to satisfy $S_pS_f = 1$ to conserve the stability margin of the system in this paper. The effect of IS on stability is only consequently analyzed.

Absolute stability is used to analyze and evaluate the stability robustness of a macro-micro teleoperation system. Absolute stability is a less conservative condition compared to passivity. Llewellyn's criterion for absolute stability is given hereinafter using hybrid matrix [38], [39].

1) h_{11} and h_{22} have no poles in the right half plane.
2) Any poles of h_{11} and h_{22} on the imaginary axis are simple with real and positive residues.
3) The following holds for all real values of system frequency ω:

$$\begin{aligned} \Re(h_{11}) &\geq 0 \\ \Re(h_{22}) &\geq 0 \\ 2\Re(h_{11})\Re(h_{22}) - \Re(h_{12}h_{21}) - |h_{12}h_{21}| &\geq 0. \end{aligned} \tag{23}$$

The last condition in (23) can be expressed as given in

$$\eta = -\cos(\angle h_{12}h_{21}) + 2\frac{\Re(h_{11})\Re(h_{22})}{|h_{12}h_{21}|} \geq 1. \tag{24}$$

Stability robustness is analyzed and evaluated by defining η as the stability index [40]. The effect of IS on stability can be known by comparing η^{IS} based on H^{IS} with η based on H. The value of η^{IS} is formulated using (16) and (24) as follows:

$$\begin{aligned} \eta^{\mathrm{IS}} &= -\cos\left(\angle h_{12}^{\mathrm{IS}}h_{21}^{\mathrm{IS}}\right) + 2\frac{\Re\left(h_{11}^{\mathrm{IS}}\right)\Re\left(h_{22}^{\mathrm{IS}}\right)}{\left|h_{12}^{\mathrm{IS}}h_{21}^{\mathrm{IS}}\right|} \\ &= -\cos\left[\angle\frac{h_{12}h_{21}}{(1+h_{22}Z_c^{\mathrm{IS}})^2}\right] \\ &\quad + 2\frac{\Re\left(\frac{h'_{11}}{1+h_{22}Z_c^{\mathrm{IS}}}\right)\Re\left(\frac{h_{22}}{1+h_{22}Z_c^{\mathrm{IS}}}\right)}{\left|\frac{h_{12}h_{21}}{(1+h_{22}Z_c^{\mathrm{IS}})^2}\right|}. \end{aligned} \tag{25}$$

If the performance of the teleoperation system is close to transparent, h_{22} becomes nearly zero and η^{IS} can be approximated by

$$\begin{aligned} \eta^{\mathrm{IS}} &\cong -\cos(\angle h_{12}h_{21}) + 2\frac{\Re\left(h'_{11}\right)\Re(h_{22})}{|h_{12}h_{21}|} \\ &= -\cos(\angle h_{12}h_{21}) + 2\frac{\Re(h_{22})}{|h_{12}h_{21}|} \\ &\quad \times \Re\left[h_{11} + (h_{11}h_{22} - h_{12}h_{21})Z_c^{\mathrm{IS}}\right] \\ &= -\cos(\angle h_{12}h_{21}) + 2\frac{\Re(h_{22})}{|h_{12}h_{21}|} \\ &\quad \times \left\{\Re(h_{11}) + \Re\left[(h_{11}h_{22} - h_{12}h_{21})Z_c^{\mathrm{IS}}\right]\right\}. \end{aligned} \tag{26}$$

As a result, η^{IS} is increased when $\Re[(h_{11}h_{22} - h_{12}h_{21})Z_c^{IS}] > 0$. Additional detail is also presented and analyzed for the PP and FP control architectures.

1) PP Control Architecture: Equation (27) is obtained from (20)

$$h_{11}h_{22} - h_{12}h_{21} = \frac{(1+C_5)Z_{cm}}{(1+C_6)Z_{cs}}. \tag{27}$$

Stability robustness is increased because it is clear that $\Re[(h_{11}h_{22} - h_{12}h_{21})Z_c^{IS}] > 0$ for PP control architecture with IS.

2) FP Control Architecture: The equation $h_{11}h_{22} - h_{12}h_{21}$ is derived from (22) as follows:

$$h_{11}h_{22} - h_{12}h_{21} = \frac{(1 + C_5)Z_{cm} + S_p S_f C_1 C_2}{(1 + C_6)Z_{cs}}. \tag{28}$$

In this case, $\Re[(h_{11}h_{22} - h_{12}h_{21})Z_c^{IS}]$ is also larger than zero; hence, stability robustness also increases.

In this regard, it is to be noted that, for in-depth analysis, the perception performance and the stability analyses should be done in the frequency domain. This is possible by substituting second-order LTI models of master and slave (e.g., $Z_m = m_m s^2 + b_m s + k_m$ for the master) by putting $j\omega$ into s in (19)–(28). We did similar work in [36] to derive the analytical stability criteria. However, in this paper, we have performed simulations with various virtual soft tissues which are presented in the supplement. The authors, nevertheless, left the frequency-domain analysis of the effect of the IS in the perception and stability for our next study.

This proposed IS method increases the detection ability while the stability robustness is also increased. However, the readers should note that an increase of the detection ability usually, but not always, decreases the transparency as is evident by $(Z_{to}^{IS} - Z_e) \gg (Z_{to} - Z_e)$. Therefore, the transparency/stability trade-off is still maintained with the IS method.

V. Psychophysical Experiments

Psychophysical experiments [29], [36] have been conducted to explain the physical meaning of the proposed kinesthetic perception and to show its effectiveness in comparing the detection and discrimination abilities of human operators for different force-feedback schemes.

In addition, we believe that psychophysical experiments are an efficient way to judge the performance of human-in-the-loop systems due to human involvement. Also, since our proposed metrics involve the low-pass-filtered derivatives of transmitted impedance with respect to the environment impedance, it is very difficult to compute the accurate derivatives of impedance in real-world situations using experimental data, which is an obvious demerit of traditional experimental methods in these cases. Hence, psychophysical experiments become all the more important in these cases to validate our approach using the concepts of AL and JND, which form the basis behind our proposed indices.

A. Participants

For both these experiments, six subjects of different backgrounds and gender, falling under the age group of 21 to 29 years, are chosen to maintain the generality of the experiments. Two of them are from technical background with no knowledge of haptics or psychophysics, while the others are familiar with haptics. Five of the subjects are males while one is female. All of the subjects were right handed by self-report.

B. Apparatus

Two kinds of psychophysical experiments have been conducted. One of them is the test of detection ability while the other is the test of discrimination ability. The experimental setup is shown in Fig. 6. The human subject manipulates the master device which is a PHANToM Premium in this case. The virtual slave manipulator is interacting with a virtual wall as the environment. The teleoperation setup implemented using Visual C++ and GUIs for detection test and discrimination test has been made to interact with the virtual environment as shown in Fig. 7(a) and (b), respectively.

For the detection test, as shown in Fig. 7(a), there is one virtual wall, and the subjects are asked to respond according to whether they can detect the wall or not. The default color of the wall is red, but it turns blue as soon as the end-effector of the virtual slave manipulator touches the wall. The discrimination

Fig. 6. Psychophysical experiment setup.

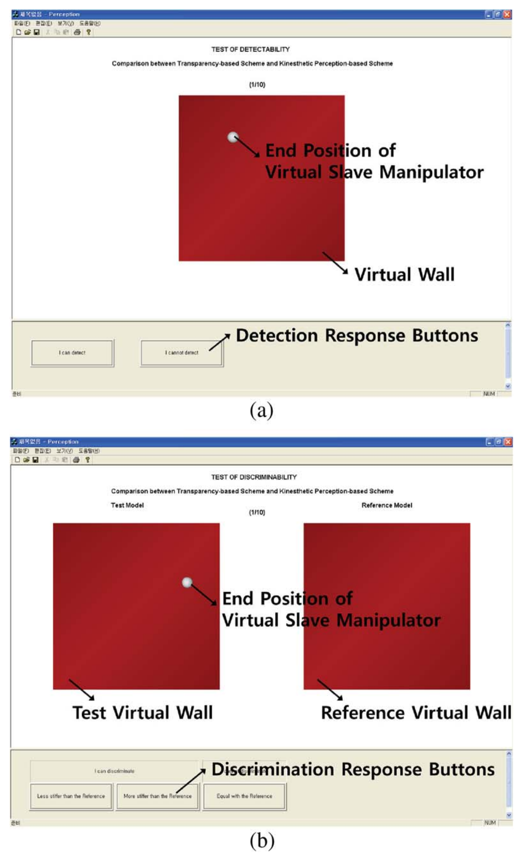

Fig. 7. GUI of psychophysical experiment. (a) For the test of detection ability. (b) For the test of discrimination ability.

test, however, has two virtual walls. The subjects are asked to discriminate between these two walls based on the haptic information that is fed back to the subject. The haptic update rate was fixed at 1 kHz for the PHANToM haptic device. The experiments were designed according to within-subject design for cost efficiency and maintaining uniformity, and the experimental procedure design has been verified by several experts in the field.

It is to be noted that the subjects could visually detect when the virtual slave contacted the virtual wall because of the color change of the wall during contact and could also hear the PHANToM motor noise. These visual and auditory effects were present for all parts of the experiments and hence do not affect the comparison of experimental results because our objective is not to find the exact values of AL and JND for human subjects but to compare the performance of various control schemes using the indices defined under the same conditions. It is also to be noted that the human subject responds according to the force feedback from the PHANToM which depends not only on the impedance of the environment but also on the insertion depth and velocity of the PHANToM end-effector. However, these aspects are left to the intuition of the human subject to make the process seem natural and the response more humancentric. Also, the choice of grip of the PHANToM as well as the choice of the right or left hand is left on the intention of the human subject based on the feeling of maximum perception of the subject to reduce the number of human factors to be analyzed. The subjects were given a detailed tutorial about the experiment in the beginning and were provided a small training session with the PHANToM to get them familiarized with that.

TABLE I
EXPERIMENTAL RESULT FOR TEST OF DETECTION ABILITY AND DISCRIMINATION ABILITY: AL AND JND

	100% Force Feedback	80% Force Feedback
AL	16.5 N/m	20.22 N/m
JND	6.975%	12.625%

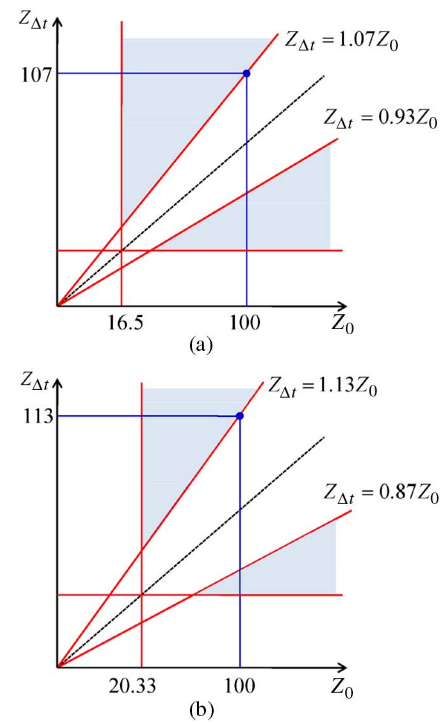

Fig. 8. Kinesthetic perception region of psychophysical experiment results. (a) Case of 100% force feedback. (b) Case of 80% force feedback. The values are obtained from Table I, and the figure is drawn based on Fig. 4 to obtain a mutual comparison.

TABLE II
EXPERIMENTAL RESULT FOR TEST OF DETECTION ABILITY AND DISCRIMINATION ABILITY: AL AND JND

	100% Force Feedback	80% Force Feedback
$M_{detection}$	1	0.81
$M_{discrimination}$	1	0.55
$PI_{perception}$	0.25	0.1594

C. Procedure

Each subject has to perform the experiments for three different *cases* where each case is divided into two *series*, such as ascending series and descending series, which are generally defined in the method of limits [29]. The three cases differ according to the different lower limits for the ascending series and different upper limits for the descending series and the variable step sizes which vary from case to case so as to rule out any possibility of intelligent guesses. Also, the cases and the series are all randomized so as to minimize the human response bias.

All the six *trials* (three cases multiplied by two series) are repeated for two kinds of force-feedback system such as 100% force feedback and 80% force feedback of environment force. This implies that two kinds of FP controllers, one with the force scaling factor 1 (100% force feedback) and the other with the force scaling factor 0.8 (80% force feedback), have been used. Therefore, each subject has to perform a total of 12 trials for the experiment to test the detection ability as well as another 12 trials for the experiment to test the discrimination ability.

D. Method

1) Test of Detection Ability: The test of detection ability is designed in such a way that a human subject who is holding the PHANToM is asked to interact with the virtual wall which is known as the *test model* and respond as to whether he or she can detect the impedance of the environment. Each subject has to perform the experiments for three different *cases* where each case is divided into two *series* such as ascending series and descending series. The three *cases* differ according to the different lower limits for the ascending *series* and different upper limits for the descending *series* and the variable step sizes which vary from *case* to *case* so as to rule out any possibility of intelligent guesses. Also, the *cases* and the *series* are all randomized so as to minimize the human response bias. The points at which the response changes from *cannot detect* to *can detect* for ascending series or vice versa for descending series are marked as transition points. The method of limits is used to calculate the AL for the subjects [29].

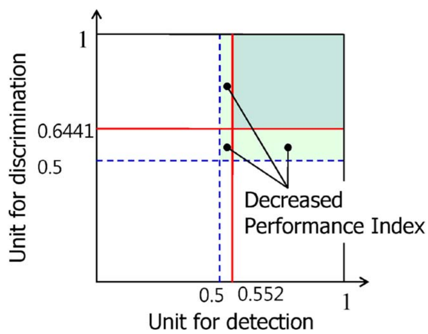

Fig. 9. Change of the performance index for kinesthetic perception in psychophysical experiment. The values are obtained from Table II and (14), and the figure is drawn based on Fig. 5 to obtain a mutual comparison.

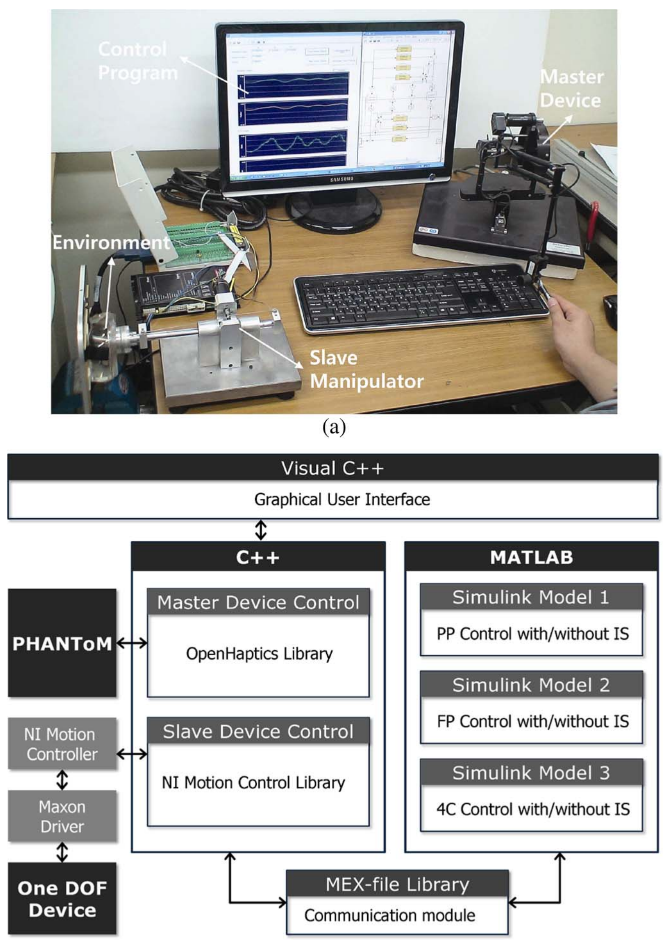

Fig. 10. Experimental setup. (a) System configuration. (b) Hardware and software architecture.

2) Test of Discrimination Ability: The GUI for the test of discrimination ability has two virtual walls, one of which is called the *test model* and the other is called the *reference model*. Each subject is asked to respond if he or she can discriminate between the test model and the reference model. Every subject has to perform the experiments for three different *cases* in which the reference models have three different environment impedances. The reference model impedances are chosen uniformly such as $Z_e = 1 + 50/s$, $Z_e = 1 + 200/s$, and $Z_e = 1 + 500/s$. For each of these reference models, there are two kinds of *series* known as ascending *series* and descending *series* which are similar to that of the test of detection. The method of limits is also used to calculate the JND for the subjects [29].

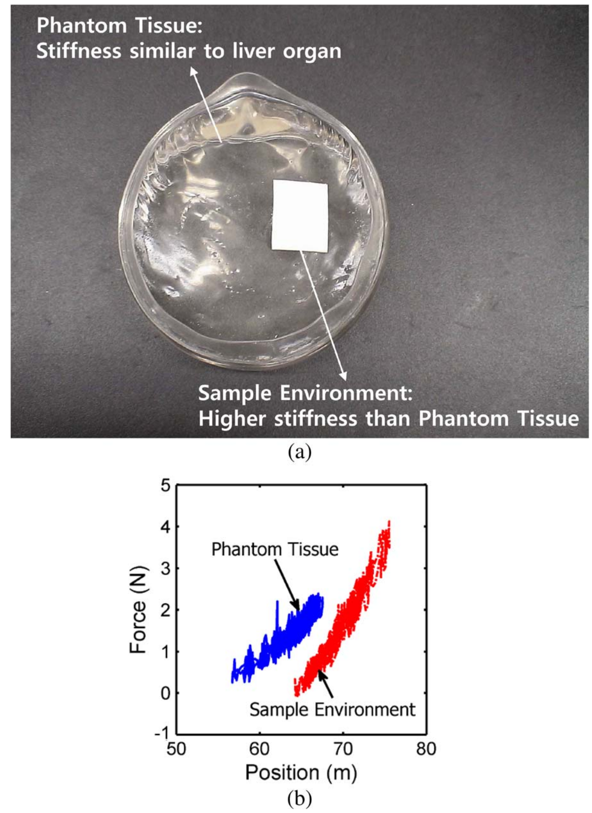

Fig. 11. Samples of two types of soft environment. (a) Phantom tissue and sample environment. (b) Characteristics of soft environments.

E. Result

Psychophysical experiment results for the test of detection ability and the test of discrimination ability are summarized in Table I using the AL and the JND. The JND is calculated using experimental results of the DL and the stiffness intensity of references, and it is expressed as percentage in this paper. In the case of 80% force feedback, both the AL and the JND are increased compared with 100% force-feedback system. Therefore, it becomes more difficult to detect and to discriminate softer environments. This experimental result can be explained easily using the proposed kinesthetic perception region as shown in Fig. 8. Please note that Fig. 8 is obtained from the measured values given in Table I and is based on Fig. 4. Kinesthetic perception region of 80% force-feedback system, shown in Fig. 8(b), is smaller than that of 100% force-feedback system shown in Fig. 8(a).

Kinesthetic perception region can be compared quantitatively using the proposed performance index for kinesthetic perception. If it is assumed that both $M_{\text{detection}}$ and $M_{\text{discrimination}}$ of the 100% force-feedback system are unity, $M_{\text{detection}}$ and $M_{\text{discrimination}}$ of the 80% force-feedback system are calculated as 0.81 and 0.55, respectively, using Table I by taking the ratio of the AL and the JND of the 80% force-feedback case to that of the 100% force-feedback case. Fig. 9 shows the

TABLE III
EXPERIMENT RESULT OF THE DETECTION ABILITY ENHANCEMENT FOR CONTROL ARCHITECTURES WITH AND WITHOUT IS WHEN $AL_e = 1$ AND $S_p = 1/3$

		Four-channel			Position-position			Force-position		
		Stiffness	$M_{detection}$	AL	Stiffness	$M_{detection}$	AL	Stiffness	$M_{detection}$	AL
Phantom Tissue	k_e	15.6970	N/D	1	15.6970	N/D	1	15.6970	N/D	1
	k_{to}	15.3060	0.9750	1.0255	10.1380	0.6459	1.5483	643.5800	41.0002	0.0244
	k_{to}^{IS}	47.0240	2.9957	0.3338	30.2290	1.9258	0.5193	672.2800	42.8286	0.0233
Enhancement		3.0723			2.9818			1.0446		

quantitative change of kinesthetic perception performance based on Table II. As a result, the kinesthetic perception ability of the 80% force-feedback system is decreased by about 32.23% when compared with the 100% force-feedback system. Please note that $\mathrm{PI}_{\mathrm{perception}}$ is calculated using (14), and then, Fig. 9 is represented using (14) and Table II, similar to Fig. 5. Therefore, we can quantify and compare the kinesthetic perception ability of a certain force-feedback system with the others using the proposed kinesthetic perception region and the performance index shown in Figs. 4 and 5, respectively.

VI. EXPERIMENT WITH PHANTOM SOFT TISSUES

A. Experimental Setup

Experiments were performed to analyze the IS control method in enhancing the perception of soft tissues. An experimental setup, as shown in Fig. 10(a), was prepared using PHANToM as the master device and a one-degree-of-freedom (DOF) mechanical device as the slave manipulator. National Instruments (NI) Motion Controller was used together with Maxon Motor Driving Circuit to control the slave manipulator. The control program was run using a GUI with constant interaction between C language and MATLAB Simulink. The software and hardware architecture of the experimental setup is shown in Fig. 10(b). As shown in the figure, the PHANToM master device communicates with the OpenHaptics Library for its control while the 1-DOF slave device communicates with its motor drivers and motion controller via NI Motion Control Library in C++. All these peripherals communicate with the control algorithm programmed in MATLAB Simulink via the communication module of MEX-file Library. Therefore, this system gives the advantage of the versatility of using MATLAB Simulink for control algorithms while using the merits of C++ for controlling the hardware peripherals. A phantom tissue was prepared as the viscoelastic soft tissue environment as shown in Fig. 11(a). The tissue was made of 1 : 1 solution of solvent and hardener to create an environment stiffness of several kilopascals and to present approximately liverlike behavior. Another sample environment was made from sponge whose stiffness is a little higher than the phantom tissue. Characteristics of the environments are shown in Fig. 11(b). Combination of the two environments, as shown in Fig. 11, represents the behavior of a polyp in the liver. This setup was used to perform experiments to check the discrimination ability of various control architectures. Position-scaling factor S_p was set to 1/3.

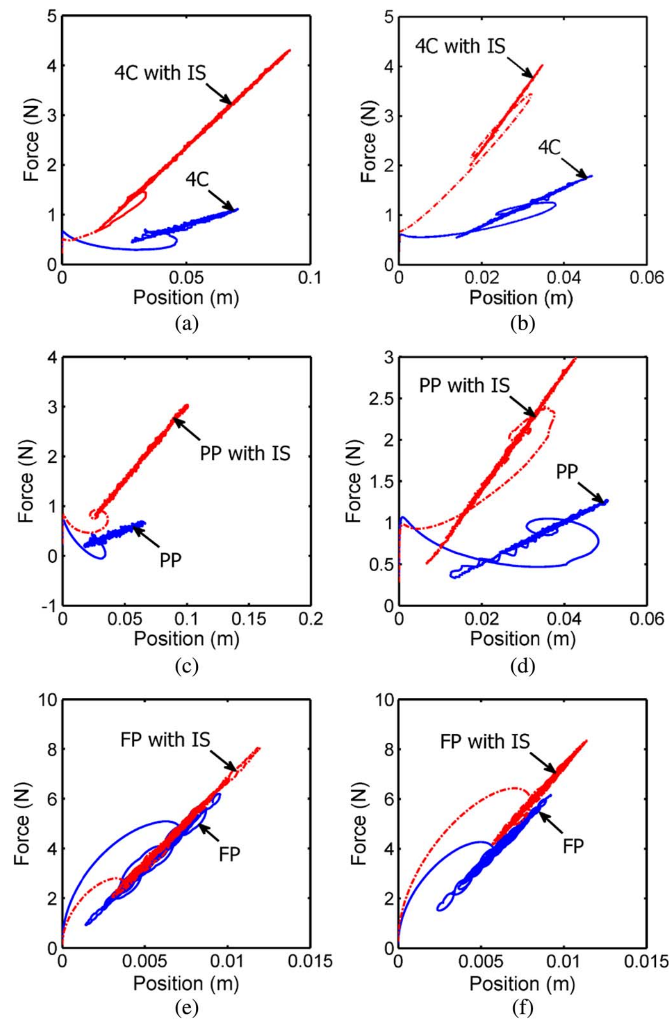

Fig. 12. Experimental results of position–force graph using 4C controller with (a) phantom tissue and (b) sample environment, PP controller with (c) phantom tissue and (d) sample environment, and FP controller with (e) phantom tissue and (f) sample environment.

B. Experiment Results: Detection

Experiment results of the detection threshold for phantom tissue are shown in Table III which are calculated from the data in Figs. 11(b) and 12(a), (c), and (e). Only stiffness is considered for the impedance to eliminate a noise from the numerical calculation of velocity and acceleration for the viscosity and the inertia, respectively. The metric for the detection ability $M_{\mathrm{detection}}$ is calculated using (12), and then, AL is calculated as the inverse of $M_{\mathrm{detection}}$ under the assumption that $AL_e = 1$. It is to be understood that our proposed metrics involve the

TABLE IV
EXPERIMENT RESULT OF THE ENHANCEMENT OF THE DISCRIMINATION ABILITY FOR THE CONTROL ARCHITECTURES WITH AND WITHOUT IS WHEN $JND_e = 1$ AND $S_p = 1/3$

		Four-channel			Position-position			Force-position		
		Stiffness	$M_{discrimination}$	JND	Stiffness	$M_{discrimination}$	JND	Stiffness	$M_{discrimination}$	JND
Environments	k_{e1}	15.6970	N/D	1	15.6970	N/D	1	15.6970	N/D	1
	k_{e2}	38.8570			38.8570			38.8570		
Without IS	k_{to1}	15.3060	1.0207	0.9797	10.1380	0.9334	1.0713	643.5800	0.0213	47.0314
	k_{to2}	38.3570			24.1000			663.7700		
With IS	k_{to1}^{IS}	47.0240	0.9857	1.0146	30.2290	0.8838	1.1315	672.2800	0.0556	17.9857
	k_{to2}^{IS}	115.4100			69.6480			727.4300		
Enhancement		0.9656			0.9469			2.6149		

H_2 norm of the low-pass-filtered derivatives of transmitted impedance with respect to the environment impedance, which is very difficult to compute accurately in real-world situations using experimental data. Hence, we use the obvious L_2 norm instead, for our experimental purposes. The psychophysical experiments, however, can deal with this limitation as it is based on the direct measurement of AL and JND on which our indices are based.

The detection threshold decreased for all the control architectures when the IS method is used. The 4C control architecture shows the highest enhancement ratio, and the FP control architecture has the smallest enhancement ratio as expected.

C. Experiment Results: Discrimination

Figs. 11 and 12 are used to quantify the discrimination ability. Table IV shows the result of the discrimination ability for various control architectures with and without IS. The goal is to discriminate between the two kinds of environment. $M_{\text{discrimination}}$ is calculated as follows as defined in (13):

$$M_{\text{discrimination}} = \frac{\Delta k_{to}^{(\text{IS})} / k_{to1}^{(\text{IS})}}{\Delta k_e / k_{e1}}. \tag{29}$$

With the assumption that $JND_e = 1$, the JND of each controller is calculated as $1/M_{\text{discrimination}}$. As explained earlier, please note the use of numerical ratio with L_2 norm, as it is very difficult to compute the derivatives of the impedances in real-world situations using the low-pass-filtered H_2 norm, as given in our proposed indices.

The discrimination ability of the 4C controller does not change when the IS method is used. In the case of PP controller, there is a small decrease in the discrimination ability. However, the ability increases largely for the FP controller. The discrimination ability is enhanced only for the FP controller when the IS method is used. This confirms the simulation results.

The results of Tables III and IV are explained using the proposed performance index for kinesthetic perception. Fig. 13 shows both the change of the detection ability and the discrimination ability using the unified kinesthetic perception region illustrated in Fig. 5. M_1 and M_2 are calculated using (14). The area of this region is the quantitative index for the performance. For all the control architectures, the kinesthetic perception region related to detection increased. The kinesthetic

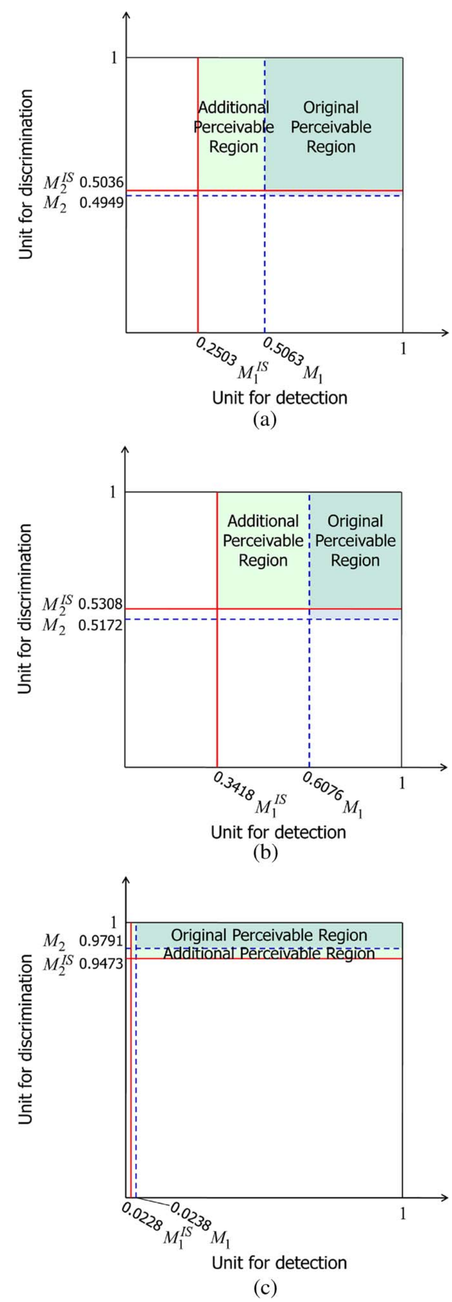

Fig. 13. Change of the performance index for kinesthetic perception in the experiment with phantom soft tissues. (a) 4C controller. (b) PP controller. (c) FP controller.

TABLE V
PERFORMANCE INDEX FOR KINESTHETIC PERCEPTION OF EXPERIMENT RESULT

	Four-channel	Position-position	Force-position
	$PI_{perception}$	$PI_{perception}$	$PI_{perception}$
Without IS	0.2494	0.1894	0.0203
With IS	0.3722	0.3088	0.0515
Enhancement	1.4923	1.6300	2.5325

perception region related to discrimination increased only in the FP controller.

Kinesthetic perception ability is summarized in Table V based on the experiment results shown in Tables III and IV. Although $\mathrm{PI}_{\mathrm{perception}}$ of the FP controller is the lowest, the enhancement ratio is the highest because the discrimination ability is enhanced only for the FP controller. Although the enhancement ratio of the 4C control architecture is the lowest, it has the highest kinesthetic perception ability.

Only the stiffness is considered in this paper to model the environment impedance because it is quite difficult in practice to estimate the nonlinear and time-varying environment impedance including the inertia and viscosity terms. The experimental results, however, clearly show the enhancement of the detection and the discrimination abilities of the developed IS method.

VII. CONCLUSION

This paper has analyzed the effect of IS control method on the perception of soft tissues in macro-micro teleoperation. The generalized teleoperation architecture is modified by adding an IS compensator, and to study its effects on the perception of soft tissues, kinesthetic perception is studied in this paper in the context of microsurgical teleoperation. Two methods are identified for enhancing the kinesthetic perception:

1) increase of Z_{to}/Z_e in relation to AL to detect smaller impedance in the environment;
2) increase of $(\Delta Z_{to}/Z_{to})/(\Delta Z_e/Z_e)$ in relation to the JND to discriminate smaller relative changes in the impedance of the environment.

A new performance index is proposed to define the kinesthetic perception quantitatively based on the two enhancement methods. The effect of the IS control method on the perception of soft tissues is then analyzed for conventional teleoperation architectures based on this newly developed index while the stability is analyzed using Llewellyn's absolute stability criteria. The IS compensator increases the stability robustness of the PP and the FP control architectures as the position-scaling factor decreases. The stability robustness of the 4C controller with IS is nearly unchanged because it is almost transparent.

Psychophysics experiments are, at first, performed which show the effectiveness of the proposed index of kinesthetic perception. Experiments are then conducted to analyze the effect of IS on the perception of soft tissues based on this proven index and to verify the results. The results show that the effects of IS on the operator's kinesthetic perception vary with different types of teleoperation control architectures. The PP controller with IS increases only the detection ability while the FP controller with IS enhances only the discrimination ability. The kinesthetic perception, which includes both the detection as well as the discrimination abilities, of the PP controller is much better than that of the FP controller. The 4C control architecture shows similar results with that of the PP control architecture. However, the enhancement ratio of the FP control is the highest. Hence, task-specific control architectures should be selected by weighing the importance of the detection ability and the discrimination ability for a particular application.

Therefore, as a topic of extensive future work, possibilities of the development of a novel control scheme would be studied which might increase both the detection and discrimination abilities to solve this tradeoff for all the controllers while maintaining the system stability.

REFERENCES

[1] J. W. Hill and J. F. Jensen, "Telepresence technology in medicine: Principles and applications," *Proc. IEEE*, vol. 86, no. 3, pp. 569–580, Mar. 1998.

[2] C. R. Wagner, N. Stylopoulos, P. G. Jackson, and R. D. Howe, "The benefit of force feedback in surgery: Examination of blunt dissection," *Presence: Teleoperators Virtual Environ.*, vol. 16, no. 3, pp. 252–262, Jun. 2007.

[3] M. C. Cavusoglu, A. Sherman, and F. Tendick, "Design of bilateral teleoperation controllers for haptic exploration and telemanipulation of soft environments," *IEEE Trans. Robot. Autom.*, vol. 18, no. 4, pp. 641–647, Aug. 2002.

[4] G. De Gersem, H. Van Brussel, and F. Tendick, "Reliable and enhanced stiffness perception in soft-tissue telemanipulation," *Int. J. Robot. Res.*, vol. 24, no. 10, pp. 805–822, Oct. 2005.

[5] J. Yan and S. E. Salcudean, "Teleoperation controller design using H_∞-optimization with application to motion-scaling," *IEEE Trans. Control Syst. Technol.*, vol. 4, no. 3, pp. 244–258, May 1996.

[6] S. Khan, A. Sabanovic, and A. O. Nergiz, "Scaled bilateral teleoperation using discrete-time sliding-mode controller," *IEEE Trans. Ind. Electron.*, vol. 56, no. 9, pp. 3609–3618, Sep. 2009.

[7] R. Taylor, P. Jensen, L. Whitcomb, A. Barnes, R. Kumar, D. Stoianovici, P. Gupta, Z. Wang, E. deJuan, and L. Kavoussi, "A steady-hand robotic system for microsurgical augmentation," *Int. J. Robot. Res.*, vol. 18, no. 12, pp. 1201–1210, Dec. 1999.

[8] M. C. Cavusoglu, F. Tendick, M. Cohn, and S. S. Sastry, "A laparoscopic telesurgical workstation," *IEEE Trans. Robot. Autom.*, vol. 15, no. 4, pp. 728–739, Aug. 1999.

[9] F. Tendick, S. S. Sastry, R. S. Fearing, and M. Cohn, "Applications of micromechatronics in minimally invasive surgery," *IEEE/ASME Trans. Mechatronics*, vol. 3, no. 1, pp. 34–42, Mar. 1998.

[10] Z. Lu, P. C. Y. Chen, and W. Lin, "Force sensing and control in micromanipulation," *IEEE Trans. Syst., Man, Cybern. C, Appl. Rev.*, vol. 36, no. 6, pp. 713–724, Nov. 2006.

[11] J. E. Colgate, "Robust impedance shaping telemanipulation," *IEEE Trans. Robot. Autom.*, vol. 9, no. 4, pp. 374–384, Aug. 1993.

[12] H. Kobayashi, "A scaled teleoperation-time scaling problem," *Adv. Robot.*, vol. 8, pp. 173–183, 1994.

[13] P. Malysz and S. Sirouspour, "Nonlinear and filtered force/position mappings in bilateral teleoperation with application to enhanced stiffness discrimination," *IEEE Trans. Robot.*, vol. 25, no. 5, pp. 1134–1149, Oct. 2009.

[14] D. Botturi, M. Vicentini, M. Righele, and C. Secchi, "Perception-centric force scaling in bilateral teleoperation," *Mechatronics*, vol. 20, no. 7, pp. 802–811, Oct. 2010.

[15] S. Yamakawa, H. Fujimoto, S. Manabe, and Y. Kobayashi, “The necessary conditions of the scaling ratio in master–slave systems based on human difference limen of force sense,” *IEEE Trans. Syst., Man, Cybern. A, Syst., Humans*, vol. 35, no. 2, pp. 275–282, Mar. 2005.
[16] N. Ando, P. Korondi, and H. Hashimoto, “Networked telemicromanipulation systems “Haptic Loupe”,” *IEEE Trans. Ind. Electron.*, vol. 51, no. 6, pp. 1259–1271, Dec. 2004.
[17] S. Katsura, Y. Matsumoto, and K. Ohnishi, “Realization of “Law of Action and Reaction” by multilateral control,” *IEEE Trans. Ind. Electron.*, vol. 52, no. 5, pp. 1196–1205, Oct. 2005.
[18] S. Katsura, K. Ohnishi, and K. Ohishi, “Transmission of force sensation by environment quarrier based on multilateral control,” *IEEE Trans. Ind. Electron.*, vol. 54, no. 2, pp. 898–906, Apr. 2007.
[19] S. Katsura and K. Ohnishi, “A realization of haptic training system by multilateral control,” *IEEE Trans. Ind. Electron.*, vol. 53, no. 6, pp. 1935–1942, Dec. 2006.
[20] T. Shimono, S. Katsura, and K. Ohnishi, “Abstraction and reproduction of force sensation from real environment by bilateral control,” *IEEE Trans. Ind. Electron.*, vol. 54, no. 2, pp. 907–918, Apr. 2007.
[21] T. Slama, A. Trevisani, D. Aubry, R. Oboe, and F. Kratz, “Experimental analysis of an Internet-based bilateral teleoperation system with motion and force scaling using a model predictive controller,” *IEEE Trans. Ind. Electron.*, vol. 55, no. 9, pp. 3290–3299, Sep. 2008.
[22] I. Peterlik and J. Filipovic, “Distributed construction of configuration spaces for real-time haptic deformation modeling,” *IEEE Trans. Ind. Electron.*, vol. 58, no. 8, pp. 3205–3212, Aug. 2011.
[23] B. Yalcin and K. Ohnishi, “Stable and transparent time delayed teleoperation by direct acceleration waves,” *IEEE Trans. Ind. Electron.*, vol. 57, no. 9, pp. 3228–3238, Sep. 2010.
[24] E. B. V. Poorten, Y. Kokokohji, and T. Yoshikawa, “Stability analysis and robust control for fixed-scale teleoperation,” *Adv. Robot.*, vol. 20, no. 6, pp. 681–706, Jun. 2006.
[25] E. V. Poorten, T. Kanno, and Y. Yokokohji, “Robust variable-scale bilateral control for micro teleoperation,” in *Proc. IEEE Int. Conf. Robot. Autom.*, 2008, pp. 655–662.
[26] K. B. Fite, J. E. Speich, and M. Goldfarb, “Transparency and stability robustness in two-channel bilateral teleoperation,” *Trans. ASME, J. Dyn. Syst. Meas. Control*, vol. 123, pp. 400–407, 2001.
[27] M. Boukhnifer and A. Ferreira, “H_∞ loop shaping bilateral controller for a two-fingered tele-micromanipulation system,” *IEEE Trans. Control Syst. Technol.*, vol. 15, no. 5, pp. 891–905, Sep. 2007.
[28] D. A. Lawrence, “Stability and transparency in bilateral teleoperation,” *IEEE Trans. Robot. Autom.*, vol. 9, no. 5, pp. 624–637, Oct. 1993.
[29] G. A. Gescheider, *Psychophysics: The Fundamentals*. Mahwah, NJ: Lawrence Erlbaum Associates, Inc., 1997.
[30] L. A. Jones, “Kinesthetic sensing,” in *Proc. Workshop Human Mach. Haptics*, 1997, pp. 1–10.
[31] X. Wang and P. X. Liu, “Improvement of haptic feedback fidelity for telesurgical applications,” *Electron. Lett.*, vol. 42, no. 6, pp. 327–329, Mar. 2006.
[32] S. Hirche and M. Buss, “Transparent data reduction in networked telepresence and teleaction system. Part II: Time-delayed communication,” *Presence: Teleoperators Virtual Environ.*, vol. 16, no. 5, pp. 532–542, Oct. 2007.
[33] P. Hinterseer, S. Hirche, S. Chaudhuri, E. Steinbach, and M. Buss, “Perception-based data reduction and transmission of haptic data in telepresence and teleaction systems,” *IEEE Trans. Signal Process.*, vol. 56, no. 2, pp. 588–597, Feb. 2008.
[34] M. Tavakoli, A. Aziminejad, R. V. Patel, and M. Moallem, “High-fidelity bilateral teleoperation systems and the effect of multimodal haptics,” *IEEE Trans. Syst., Man, Cybern. B, Cybern.*, vol. 37, no. 6, pp. 1512–1528, Dec. 2007.
[35] H. I. Son, T. Bhattacharjee, H. R. Jung, and D. Y. Lee, “Psychophysical evaluation of control scheme designed for optimal kinesthetic perception in scaled teleoperation,” in *Proc. IEEE Int. Conf. Robot. Autom.*, 2010, pp. 5346–5351.
[36] H. I. Son, T. Bhattacharjee, and H. Hashimoto, “Enhancement in operator’s perception of soft tissues and its experimental validation for scaled teleoperation systems,” *IEEE/ASME Trans. Mechatronics*, 2010, to be published. [Online]. Available: http://ieeexplore.ieee.org/xpls/abs_all.jsp?arnumber=5605252
[37] W. E. Baker, P. S. Westine, and F. T. Dodge, *Similarity Methods in Engineering Dynamics: Theory and Practice of Scale Modeling*. New York: Hayden, 1973.
[38] S. S. Haykin, *Active Network Theory*. Reading, MA: Addison-Wesley, 1970.
[39] R. J. Adams and B. Hannaford, “Stable haptic interaction with virtual environments,” *IEEE Trans. Robot. Autom.*, vol. 15, no. 3, pp. 465–474, Jun. 1999.
[40] K. Hashtrudi-Zaad and S. E. Salcudean, “Analysis of control architectures for teleoperation systems with impedance/admittance master and slave manipulators,” *Int. J. Robot. Res.*, vol. 20, no. 6, pp. 419–445, Jun. 2001.

Hyoung Il Son (M’11) received the B.S. and M.S. degrees from the Department of Mechanical Engineering, Pusan National University, Pusan, Korea, in 1998 and 2000, respectively, and the Ph.D. degree from the Department of Mechanical Engineering, Korea Advanced Institute of Science and Technology, Daejeon, Korea, in 2010.

He is currently a Research Scientist with the Department of Human Perception, Cognition and Action, Max Planck Institute for Biological Cybernetics, Tübingen, Germany. Before joining MPI, he was a Researcher with the Institute of Industrial Science, The University of Tokyo, Tokyo, Japan, until March 2010. He was also a Senior Researcher with the Production Engineering Research Institute, LG Electronics, Pyeongtaek, Korea, from 2003 to 2005, and with the Mobile Display Center, Samsung Electronics, Cheonan, Korea, from 2005 to 2009. His research interests include haptics, teleoperation, and supervisory control of discrete event/hybrid systems.

Tapomayukh Bhattacharjee received the B.Tech. degree from the Department of Mechanical Engineering, National Institute of Technology, Calicut, India, in 2006 and the M.S. degree from the Department of Mechanical Engineering, Korea Advanced Institute of Science and Technology, Daejeon, Korea, in 2009.

He is currently a Visiting Scientist with the Cognitive Robotics Center, Korea Institute of Science and Technology, Seoul, Korea. He was a Graduate Engineer Trainee with TAL Manufacturing Solutions Ltd., Tata Motors Campus, Pune, India, from 2006 to 2007. His research interests include haptics, teleoperation, manipulation and control of humanoid redundant arm systems, and humanoid hand–arm coordination.

Hideki Hashimoto (M’89–SM’04–F’06) received the B.S., M.S., and D.Eng. degrees from the Department of Electrical Engineering, The University of Tokyo, Tokyo, Japan, in 1981, 1984, and 1987, respectively.

He joined the Institute of Industrial Science, The University of Tokyo, as a Lecturer in April 1987, where he has been an Associate Professor since July 1990. He was a Visiting Scientist with the Laboratory for Information and Decision System and Laboratory for Electromagnetic and Electronic Systems, Massachusetts Institute of Technology, Cambridge, from September 1989 to August 1990. He is an Invited Distinguished Professor with Seoul National University, Seoul, Korea, from 2009 to 2011, and a Visiting Professor with the Budapest University of Technology and Economics, Budapest, Hungary, from 2009 to 2011. His research topics are intelligent systems and robotics and control.

Dr. Hashimoto was an Administrating Committee member of the IEEE Industrial Electronics Society (IES) and Robotics and Automation Society and a Vice President of the IEEE IES and IEEE Intelligent Transportation Systems Conference (ITSC). He was the Founding General Chairman of the 1997 IEEE/ASME International Conference on Advanced Intelligent Mechatronics. He was also the Program Chairman of the IEEE/RSJ International Conference on Intelligent Robots and Systems in 2000 and a General Chairman of the IEEE ITSC in 2002.